

Nonlinear Schrödinger flow past an obstacle in one dimension

Vincent Hakim

Laboratoire de Physique Statistique, 24 rue Lhomond, 75231 Paris Cedex 05, France

(Received 19 August 1996)

The flow of a one-dimensional defocusing nonlinear Schrödinger fluid past an obstacle is investigated. Below an obstacle-dependent critical velocity, a steady dissipationless motion is possible and the flow profile is determined analytically in several cases. At the critical velocity, the steady flow solution disappears by merging with an unstable solution in a usual saddle-node bifurcation. It is argued that this unstable solution represents the transition state for emission of gray solitons. The barrier for soliton emission is explicitly computed and vanishes at the critical velocity. Above the critical velocity, the flow becomes unsteady and its characteristics are studied numerically. It is found that gray solitons are repeatedly emitted by the obstacle and propagate downstream. Upstream propagating dispersive waves are emitted concurrently. A hydraulic approximation is used to interpret these results. [S1063-651X(97)11503-3]

PACS number(s): 03.40.Gc, 42.65.Vh, 67.40.Hf

I. INTRODUCTION

The nonlinear Schrödinger (NLS) equation appears in different physical problems. It is an envelope equation for small amplitude almost monochromatic waves and it appears as such in nonlinear optics [1] and, for instance, in the study of gravity waves on deep water [2]. It also describes the condensate dynamics of a weakly interacting Bose gas [3], a subject of renewed interest [4,5]. In this latter context, two-dimensional numerical simulations of NLS flow have been performed [6–8] in order to shed some light on vortex generation by a moving charge or equivalently by a flow around an obstacle in superfluid ^4He [9]. The aim of this paper is to analyze the analogous problem of NLS flow past an obstacle in one dimension where it is more easily tractable and quite instructive.

We study the NLS equation with an added external localized repulsive potential U moving at velocity $v > 0$ and meant to represent the motion of an impurity in the NLS fluid at rest at $x = +\infty$,

$$i\partial_t A = -\partial_{xx} A - A + |A|^2 A + U(x-vt)A. \quad (1)$$

The boundary condition $A = 1$ is imposed at $x = +\infty$. Since we are interested in the finite density case, a repulsive sign has been chosen for the nonlinear term (as appropriate for the imperfect Bose gas and for defocusing optical media) so that a constant density solution is stable away from the impurity [10]. The phenomenology of Eq. (1) turns out to be similar to higher dimensions [6], vortices being replaced in one dimension by propagating localized density depression of the form [11,12]

$$A(x,t) = \frac{(c+i\lambda)^2/2 + \exp[\lambda(x-ct)]}{1 + \exp[\lambda(x-ct)]}, \quad c^2 + \lambda^2 = 2 \quad (2)$$

which we call gray solitons in the following, using a nonlinear optics terminology.

Equation (1) can be written in the frame of the moving impurity, as

$$i\partial_t A - iv\partial_x A = -\partial_{xx} A - A + |A|^2 A + U(x)A. \quad (3)$$

In this equivalent formulation, it describes the flow of a NLS fluid past an immobile obstacle [13]. In an envelope equation context, the term $v\partial_x$ also appears naturally and describes the propagation of the wave envelope at the group velocity. The specific question that we consider is the nature of the flow (i.e., steady or time-dependent) when a flow of constant density is injected at velocity v at infinity. In Sec. II, we first analyze the steady solutions of Eq. (3) and focus on three cases which can be described analytically. These are weak potentials, potentials of short range, and, on the contrary, slowly varying potentials. In every case, we find that below a critical velocity which depends on the characteristics of the potential, there is a stable steady flow solution. There also exists (at least) one unstable flow solution which we interpret as the transition state toward the creation of gray solitons. At the critical velocity, both solutions coalesce and disappear in a saddle-node bifurcation so that no steady solution exists above the critical velocity. In order to investigate what happens in this regime, we resort to numerical integration in Sec. III. It is found that gray solitons are continuously emitted in the wake of the obstacle together with upstream propagating disturbances.

II. STEADY FLOWS

We begin by analyzing the existence of time-independent solutions of Eq. (3). We look for a solution in the form $A(x) = R(x)\exp[i\phi(x)]$. This gives

$$v\partial_x R = 2\partial_x R\partial_x \phi + R\partial_{xx}\phi, \quad (4)$$

$$-vR\partial_x \phi = \partial_{xx} R - R(\phi_x)^2 + R - R^3 - U(x)R. \quad (5)$$

Equation (4) can be interpreted as the fluid conservation equation [14] and can readily be integrated once. This determines the gradient of ϕ [half the fluid velocity with our normalization of Eq. (1)] as a function of $R(x)^2$ (the local fluid density),

$$\partial_x \phi = \frac{v}{2} \left(1 - \frac{1}{R^2} \right). \quad (6)$$

Substituting Eq. (6) into Eq. (5), $R(x)$ is found to obey the equation

$$\partial_{xx}R = \frac{v^2}{4} \left(-R + \frac{1}{R^3} \right) + R^3 - R + U(x)R. \quad (7)$$

We want to find solutions $R(x)$ of Eq. (7) which tend to one at $x = \pm\infty$. Linearizing Eq. (7) for large $|x|$ as $R(x) = 1 + r(x)$, one obtains

$$\partial_{xx}r = (2 - v^2)r. \quad (8)$$

Therefore, for v larger than the sound velocity $v_s = \sqrt{2}$, there are two oscillating modes around $x = -\infty$ and two around $x = +\infty$. The annulation of the amplitudes of these four modes gives too many constraints and prevents the existence of a localized solution for a generic potential [once $r \rightarrow 1$ is imposed at $x = -\infty$ there remains no freedom in the second-order equation (7) to cancel the coefficients of the two oscillating modes around $x = +\infty$]. On the contrary, for $v < v_s$, there is only one diverging mode for $|x| \gg 1$. Once the amplitude of the divergent mode is chosen to vanish around $x = -\infty$, the amplitude of the convergent mode is a free parameter. The amplitude of the divergent mode at $x = +\infty$ is a function of this parameter and the existence of localized steady flow solutions depends on the existence of zeros of this function which is not *a priori* guaranteed. In fact, we are now going to show on several examples that localized solutions only exist for $v < v_c$, where v_c is a critical velocity which depends on the potential $U(x)$ and is strictly less than v_s .

A. Short range potentials

We start with the simple case of a potential of range short as compared to the coherence length of the NLS equation [scaled to unity in Eq. (3)] which can be treated as a (pseudo) potential δ of strength g ,

$$U(x) = g\delta(x). \quad (9)$$

This imposes a discontinuity in the derivatives of A at the origin proportional to g ,

$$\partial_x A|_{0+} - \partial_x A|_{0-} = gA(0). \quad (10)$$

For an injection speed smaller than the speed of sound at infinity $v < \sqrt{2}$, the integration of Eq. (7) gives

$$R^2 = \frac{v^2}{2} + \left(1 - \frac{v^2}{2} \right) \tanh^2 \left[\sqrt{1/2 - v^2/4} (x \pm x_0) \right], \quad x \geq 0. \quad (11)$$

The corresponding phase is obtained from Eq. (6) as

$$\begin{aligned} \phi(x) &= f(x) \\ &= \arctan \left(\frac{(2v^2 - v^4)^{1/2}}{\exp[\sqrt{2 - v^2}(x + x_0)] + v^2 - 1} \right), \quad x > 0, \\ \phi(x) &= 2f(0) - f(-x), \quad x < 0. \end{aligned} \quad (12)$$

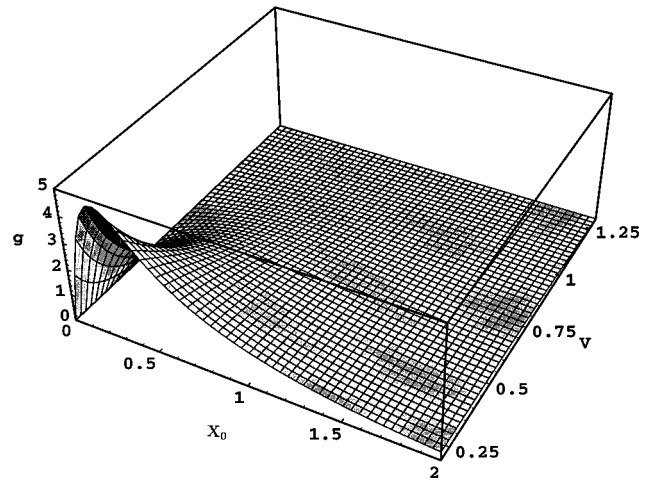


FIG. 1. The relation between x_0, v and g for $0 < x < 2$ and $0.2 < v < 1.3$. The front cut of the surface shows that for fixed v (here equal to 0.2) there are two possible x_0 for g smaller than g_m and none above.

Equations (11) and (12) can also be grouped in a single expression for $A(x, t)$ as in Eq. (2) if one prefers so.

The possible values of the constant x_0 are determined as a function of the potential strength g by the relation (10),

$$g = \sqrt{2} (1 - v^2/2)^{3/2} \frac{\tanh[\sqrt{1/2 - v^2/4} x_0]}{v^2/2 + \sinh^2[\sqrt{1/2 - v^2/4} x_0]}. \quad (13)$$

This relation is plotted in Fig. 1. For a given potential strength g , there are two possible x_0 (and therefore two possible steady flows) for each injection velocity v smaller than a potential-dependent critical velocity, $v < v_c(g)$, whereas for $v > v_c(g)$ there are none. The modulus and phase of these two solutions are shown in Figs. 2 and 3 for $g=2$ and

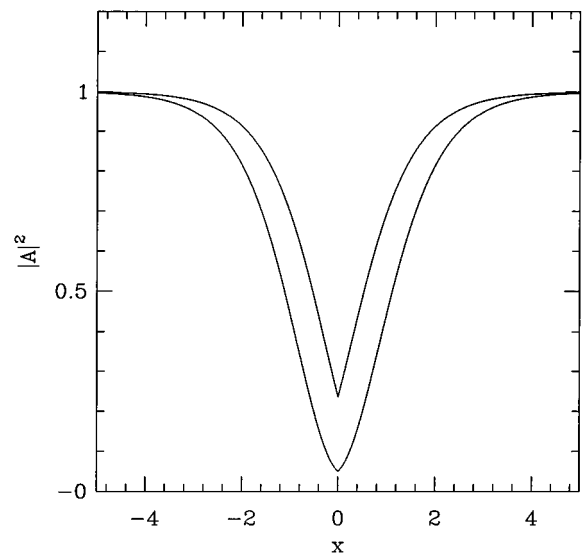


FIG. 2. The square modulus of the two time-independent solutions for a δ -potential of strength $g=2$ and flow velocity $v=0.3$ below the critical velocity ($v_c=0.41891$). The lower curve corresponds to $x_{0,-}=0.112087$ (the unstable solution) and the upper one to $x_{0,+}=0.69669$ (the stable solution).

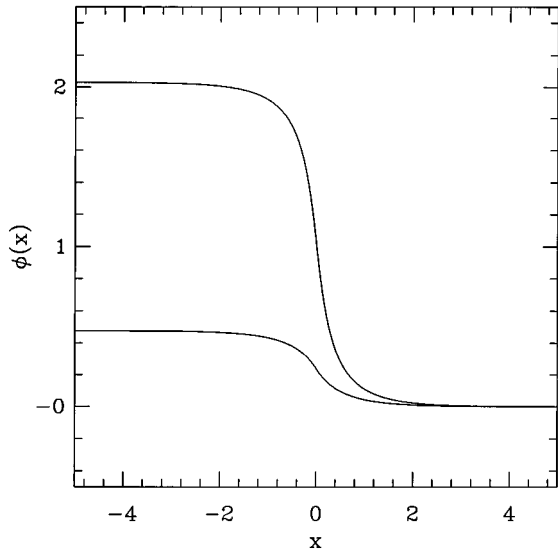


FIG. 3. The phase of the two time-independent solutions shown in Fig. 2. The upper curve corresponds to the unstable solution ($x_{0,-}$) and the lower one to the stable solution ($x_{0,+}$).

$v = 0.3$ below $v_c(2) = 0.4189$. Equation (13) determines the critical velocity v_c as a function of the potential strength g (see Fig. 4),

$$g = 4(1 - v_c^2/2) \frac{[\sqrt{1 + 4v_c^2} - (1 + v_c^2)]^{1/2}}{2v_c^2 - 1 + \sqrt{1 + 4v_c^2}}. \quad (14)$$

One obtains, for example, $v_c \approx 0.647$ for $g = 1$, $v_c \approx 0.419$ for $g = 2$, and $v_c \approx 0.304$ for $g = 3$. For a small potential strength, v_c is close to the sound velocity

$$v_c = \sqrt{2} - \frac{3}{2\sqrt{2}} g^{2/3} + \dots, \quad g \ll 1. \quad (15)$$

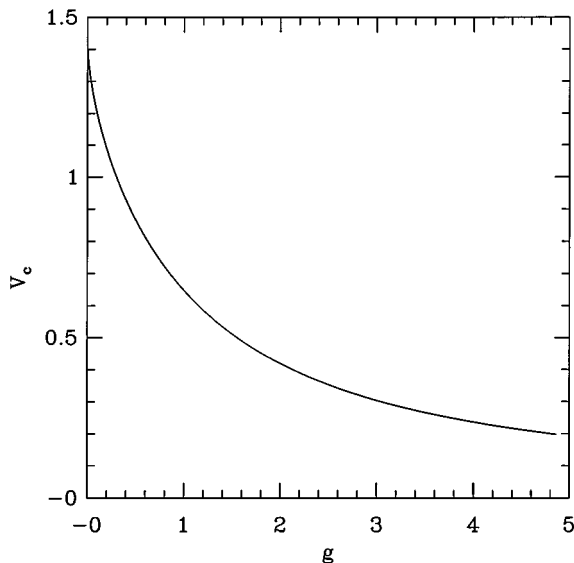


FIG. 4. The critical velocity v_c for a δ potential of strength g . A stable steady solution (as well as an unstable one) exists only below the curve $v_c(g)$.

But v_c decreases as the potential strength increases and the critical velocity tends to zero for large g ,

$$v_c \approx \frac{1}{g}, \quad g \gg 1. \quad (16)$$

The loss of steady solutions can also be obtained at a fixed velocity v (smaller than the sound speed $\sqrt{2}$) by increasing the potential strength from $g = 0$. The two solutions which exist for small potential strength merge and disappear in a usual saddle-node bifurcation at g such that $v_c(g) = v$. It should be noted that the minimum amplitude of the critical solution at the merging of the two solution branches does not vanish. So, the disappearance of time-independent solutions is not signaled in one dimension by the appearance of a phase singularity in contrast to what has been predicted for the NLS equation in higher dimensions [7].

It is instructive to look at the limiting form of the two solutions when the potential strength g tends to zero. In this case, the largest root of Eq. (13) $x_{0,+}$ tends to $+\infty$ and the corresponding solution to $A = 1$, the unperturbed flow. On the contrary, the smaller root $x_{0,-}$ tends to zero and the limiting corresponding solution is simply a gray soliton moving upstream at velocity v in the fluid referential so as to stay at a fixed position in the obstacle reference frame. The maximum of the soliton depression is on top of the repulsive potential, the less disadvantageous location. Of the two solutions which merge at the saddle node bifurcation, one is presumably stable and the other one should then be unstable on general grounds. The small- g limiting behavior leads us to guess that the stable solution corresponds to $x_{0,+}$ and the unstable one to $x_{0,-}$. This is further supported by the fact that as g increases from 0, $x_{0,+}$ decreases toward the merging value $x_{0,m}$ [15] (see Fig. 1) and the amplitude depression of the corresponding solution increases as physically expected. On the contrary, for the solution corresponding to $x_{0,-}$, $x_{0,-}$ increases toward $x_{0,m}$ and the depression amplitude decreases as the potential strength is increased.

This stability assignment can be checked by remembering that Eq. (3) is a Hamiltonian system,

$$i \partial_t A = \frac{\delta K}{\delta A^*} \quad (17)$$

with

$$K = H - vP + v[\phi(+\infty) - \phi(-\infty)]. \quad (18)$$

H and P are the Hamiltonian and momentum in the fluid reference frame,

$$H = \int dx \left\{ |\partial_x A|^2 + \frac{1}{2} (|A|^2 - 1)^2 + U(x)(|A|^2 - 1) \right\},$$

$$P = \frac{1}{2i} \int dx \{ A^* \partial_x A - A \partial_x A^* \}. \quad (19)$$

The last term in Eq. (18) imposes the appropriate boundary condition of a constant flow [16].

For a given potential strength g and injection velocity v , the steady solutions are local stationary points of K . It is numerically checked below by using the gradient dynamics

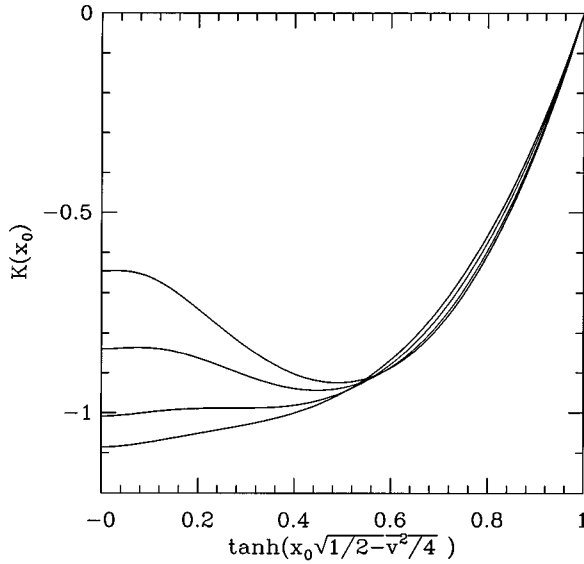


FIG. 5. The functional K evaluated for solution of the form (11) and (12) as a function of the parameter x_0 for a potential strength $g=2$ and different values of the velocity; from top to bottom: $v=0.2, 0.3, 0.41891$ (the critical velocity), 0.5 . At the critical velocity, the two nontrivial extrema disappear and the barrier height vanishes.

associated to K that the solution corresponding to $x_{0,+}$ is a local minimum of K . On the contrary, the solution corresponding to $x_{0,-}$ is an unstable saddle point of K . An appealing interpretation of the unstable solution is that it is a transition state in Eyring's sense (sometimes also called "sphaleron" [17]), i.e., that it corresponds to the smallest barrier that has to be overcome to create a gray soliton from the stable steady solution. The barrier height can be obtained by computing the value of K for a function of the form (11) and (12) using x_0 as a free parameter. One obtains

$$K(x_0) = F[\sqrt{1-v^2/2} \tanh(\sqrt{1/2-v^2/4} x_0)] - F[\sqrt{1-v^2/2}] \quad (20)$$

with

$$F[t] = \frac{2\sqrt{2}}{3} t^3 - 2\sqrt{2}t + 2v \arctan(\sqrt{2}t/v) + gt^2. \quad (21)$$

$K(x_0)$ is plotted in Fig. 5. For $v < v_c$, it has a minimum at $x_{0,+}$ and a local maximum at $x_{0,-}$. The barrier height $[K(x_{0,-}) - K(x_{0,+})]$ vanishes as v tends toward v_c . A direct numerical test of the role of the unstable solution would be interesting. One could think of transforming the deterministic equation (3) into a Langevin equation by adding noise (temperature) and friction terms. Two difficulties have to be noted, however. The first one particular to one dimension is that any amount of noise will destroy the assumed long-range order. The second one is that, in this purely classical setting, an ultraviolet cutoff has to be introduced in order to avoid the Rayleigh-Jeans catastrophe. Another interesting possibility may be to test the response of the steady flow to periodic perturbations, like sound waves.

B. Weak potentials

The steady solutions of Eq. (3) can be analyzed quite generally if the obstacle potential is weak. It turns out that the bifurcation and loss of steady solution for a generic weak potential are also described by the δ -function pseudopotential bifurcation as we now show, the reason being that in this case the bifurcation happens below but close to $v_s = \sqrt{2}$ for which the extension of the gray soliton becomes very large.

For a weak potential, one solution can be obtained perturbatively by expanding Eq. (7) around the unperturbed steady flow as

$$R = 1 + r^{(1)} + \dots \quad (22)$$

The first-order term satisfies

$$\partial_{xx} r^{(1)} = (2 - v^2) r^{(1)}(x) + U(x). \quad (23)$$

For $v < \sqrt{2}$, this gives

$$r^{(1)}(x) = - \int_{-\infty}^{+\infty} \frac{dy}{2\sqrt{2-v^2}} \exp(-\sqrt{2-v^2}|x-y|) U(y). \quad (24)$$

Besides this first solution, another perturbative solution is obtained by expanding the flow around a gray soliton stationary at position x_p in the obstacle frame

$$R(x) = R_0(x - x_p) + s^{(1)}(x) + \dots \quad (25)$$

with the gray soliton amplitude given by

$$R_0(x - x_p) = \left\{ \frac{v^2}{2} + \left(1 - \frac{v^2}{2} \right) \tanh^2[\sqrt{1/2-v^2/4}(x - x_p)] \right\}^{1/2}. \quad (26)$$

$s^{(1)}(x)$ obeys the equation

$$\begin{aligned} \partial_{xx} s^{(1)} + \left[1 - 3R_0^2 + \frac{v^2}{4} \left(1 + \frac{1}{3R_0^4} \right) \right] s^{(1)}(x) \\ = U(x) R_0(x - x_p). \end{aligned} \quad (27)$$

The arbitrariness in the position x_p of the zeroth-order solution is as usual fixed by requiring that the inhomogeneous term on the right-hand side (r.h.s.) of Eq. (27) be orthogonal to the zero mode $\partial_x R_0(x - x_p)$ of the linear operator on the left-hand side (l.h.s.) (so that no secular term appears in $s^{(1)}$),

$$\int_{-\infty}^{+\infty} dx R_0(x - x_p) \partial_x R_0(x - x_p) U(x) = 0. \quad (28)$$

The two solutions (22) and (25) merge and disappear at v_c below but close to $v_s = \sqrt{2}$. The deviation of v_c from v_s can be related to the potential $U(x)$ in the following way.

Close to the sound velocity, both Eq. (22) and Eq. (25) become of small amplitude so we assume (and check self-consistently) that R deviates slightly from a constant density when the bifurcation takes place. Writing $R(x) = 1 + \rho(x)$, $v = \sqrt{2} - \eta$, the full equation (7) becomes

$$\partial_{xx} \rho = 2\sqrt{2} \eta \rho + 6\rho^2 + U(x) + \dots \quad (29)$$

The first two terms on the r.h.s. of Eq. (29) are of similar magnitude when $\rho \sim \eta$. Comparison with the l.h.s. of Eq. (29) shows that ρ varies on a long length scale proportional to $1/\sqrt{\eta}$. Introducing the rescaled quantities $\rho = \eta r$ and $x = \xi/\sqrt{\eta}$, one obtains that the bifurcation is described for a small potential U by

$$\partial_{\xi\xi} r = 2\sqrt{2}r + 6r^2 + \kappa\delta(\xi), \quad (30)$$

where the δ -potential strength is given by

$$\kappa = \frac{1}{\eta^2} \int_{-\infty}^{+\infty} d\xi U\left(\frac{\xi}{\sqrt{\eta}}\right) = \frac{1}{\eta^{3/2}} \int_{-\infty}^{+\infty} dx U(x). \quad (31)$$

Steady solutions are found to disappear at $\kappa = (2\sqrt{2}/3)^{3/2}$ by following the calculations of the preceding section for Eq. (30) or simply by noting that it corresponds to the small- g limit (15). Finally, for a weak potential the critical velocity v_c is given by [18]

$$v_c = \sqrt{2} - \frac{3}{2\sqrt{2}} \left(\int_{-\infty}^{+\infty} dx U(x) \right)^{2/3} + \text{h.o.t.} \quad (32)$$

C. Slowly varying potentials

Potentials which vary on long length scales (compared to the NLS coherence length) provide a last analytically tractable case. In order to keep track of the small parameter, we write the potential as $U(\epsilon x)$ in Eq. (3) instead of $U(x)$.

To zeroth order in ϵ , the gradient term can be neglected in Eq. (7) and the solution modulus is equal to $R_0(x)$ with

$$U(\epsilon x) = \frac{v^2}{4} \left(1 - \frac{1}{R_0^4(x)} \right) + 1 - R_0^2(x) \equiv f(v, R_0(x)). \quad (33)$$

$f(v, R)$, considered as a function of R , increases with R for small R , reaches a maximum at $R^* = (v/\sqrt{2})^{1/3}$, and then decreases to zero as R increases toward 1. So, for a given velocity, a stationary solution only exists when the maximum of the potential U_{\max} is below $f(v, R^*)$. The critical velocity is attained when $R(x) = R^*$ at U_{\max} , a condition which is simply interpreted in the hydrodynamics analogy as meaning that the local fluid velocity in the obstacle frame ($-v + 2\partial_x \phi = -v/R^2$) is equal at the potential maximum to the local sound velocity $\sqrt{2}R$. This determines the zeroth-order estimate v_0 of the critical velocity as a function of the maximum value of the potential as

$$U_{\max} = \frac{v^2}{4} - \frac{3}{2} \left(\frac{v^2}{2} \right)^{1/3} + 1. \quad (34)$$

The steady solution loss at the critical velocity can be more precisely analyzed by taking into account the gradient term to lowest order. This determines as well the ϵ correction to the critical velocity v_0 . In order to do that we assume (and again check *a posteriori*) that the stable and unstable solution merge for v_c close to v_0 and that in this range of velocity they are close to $R_0(x)$ and differ notably from it only in a boundary layer near the maximum of the potential (which we suppose located at $x=0$ for definiteness). So, we expand

$R(x)$ around $R^*(v_0)$ (which we denote simply by R^* in the following), $U(\epsilon x)$ around the maximum of the potential, and v around v_0 ,

$$R(x) = R^*(v_0) + r(x),$$

$$U(\epsilon x) = U_{\max} + \frac{U''(0)}{2} \epsilon^2 x^2 + \dots, \quad v = v_0 + \delta v. \quad (35)$$

Correspondingly, we expand $f(v, R)$ as

$$f(v, R) = f(v_0, R^*) - f_1 \delta v - f_2 \frac{r^2}{2} + \dots \quad (36)$$

with

$$f_1 \equiv -\partial_v f|_{v_0, R^*} = \frac{v_0}{2} [-1 + (2/v_0^2)^{2/3}],$$

$$f_2 \equiv -\partial_{RR} f|_{v_0, R^*} = +2 + 5(v_0)^2/R^{*6} = 12. \quad (37)$$

Substituting these expansions into Eq. (7), one obtains

$$\partial_{xx} r = \frac{R^* U''(0)}{2} \epsilon^2 x^2 + R^* f_1 \delta v + 6R^* r^2 + \dots \quad (38)$$

Comparing the magnitude of the different terms in Eq. (38), we obtain that the bifurcation takes place for $r \sim \epsilon^{2/3}$, $x \sim \epsilon^{-1/3}$, $\delta v \sim \epsilon^{4/3}$ which justifies the expansion (35). This leads us to introduce the rescaled variables

$$r = \rho \epsilon^{2/3} \left[\frac{|U''(0)|}{72R^*} \right]^{1/3}, \quad x = X \epsilon^{-1/3} [3R^* |U''(0)|]^{-1/6},$$

$$\delta v = \Delta \epsilon^{4/3} \frac{1}{2f_1} \left[\frac{|U''(0)|^2}{3R^{*2}} \right]^{1/3}. \quad (39)$$

With these variables, the equation describing the bifurcation is simply

$$\partial_{XX} \rho = \rho^2 - X^2 + \Delta \quad (40)$$

with the boundary condition $\rho \sim |X|$ for $|X| \gg 1$. For $\Delta < 0$ and $|\Delta| \gg 1$ (i.e., well below the zeroth-order critical velocity), Eq. (40) has two solutions which can be approximately described [19]. One is the above ‘‘adiabatic’’ approximation

$$\rho_+(x) = \sqrt{x^2 - \Delta}. \quad (41)$$

The other is a simple example of an internal boundary layer and describes a small gray soliton moving upstream in the fluid reference frame almost at the sound velocity so as to stand at the fixed position in the obstacle frame,

$$\rho_-(x) = \sqrt{x^2 - \Delta} - \frac{3\sqrt{|\Delta|}}{\cosh^2(X|\Delta|^{1/4}/\sqrt{2})}. \quad (42)$$

These approximations are compared to numerically determined solutions in Fig. 6. The two solutions continue to exist for all negative Δ and for positive values of Δ up to Δ_c [but, of course, they are no longer correctly described by the approximations (41) and (42), which do not even make sense

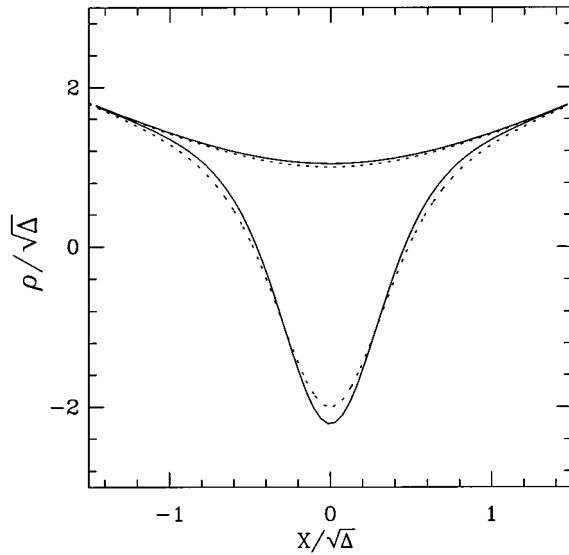


FIG. 6. The two numerical solutions of Eq. (40) for $\Delta = -10^{2/3} \approx -4.64$ (bold lines) compared to their approximate large $|\Delta|$ approximations (41) and (42) (dashed lines).

for $\Delta > 0$]. The critical value has been numerically determined to be $\Delta_c \approx 1.466$ (the two solutions are shown close to merging in Fig. 7). Therefore, taking into account the spatial variation of the potential increases the zeroth-order estimate of the critical velocity to

$$v_c = v_c^0 + 0.51 \frac{\epsilon^{4/3}}{f_1} \left[\frac{|U''(0)|}{R^*} \right]^{2/3}. \quad (43)$$

III. TIME-DEPENDENT FLOWS

Equation (3) was integrated numerically in order to test the above analytical results and study what happens above the critical velocity. We used a finite-difference semi-implicit Crank-Nicholson scheme. The obstacle was imposed at $x=0$ and the evolution was computed in the domain

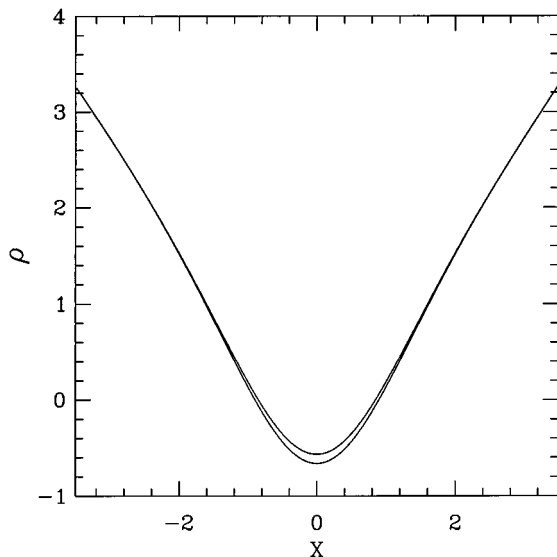


FIG. 7. The two numerical solutions of Eq. (40) for $\Delta = 1.465$ close to $\Delta_c \approx 1.466$ where they become identical and disappear.

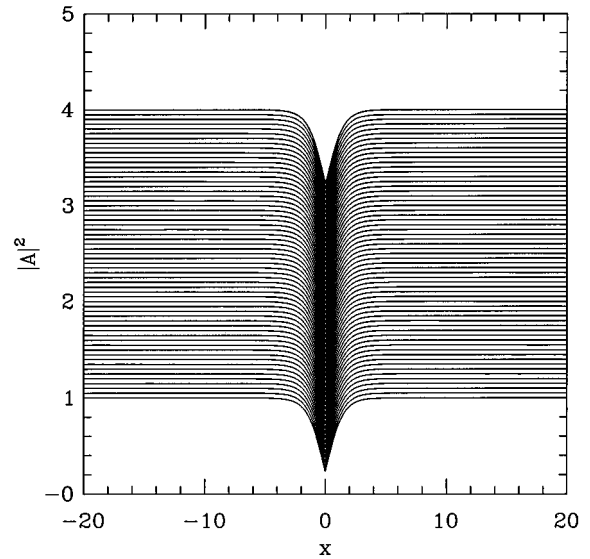


FIG. 8. Numerical integration of Eq. (3) with $v=0.3$ and a δ potential of strength $g=2$, below the critical curve ($v_c=0.41891$ for $g=2$), from $t=0$ to $t=30$. The initial condition is the steady solution (11) and (12) with $x_{0,+}=0.69669$. The solution square modulus is plotted at integer and half-integer times (shifted upward by $t/10$). The numerical integration shows that it is stable.

$-L < x < L$ with L up to 300. Most computations were carried out with a space discretization $\Delta x=0.05$ and a time discretization $\Delta t=0.01$. Some runs were performed on finer grids to check that the results were not affected in a significant way by the discretization. Dissipative terms have been added to Eq. (3) in small neighborhoods of the domain extremities in order to minimize wave reflections at the domain ends.

We first consider the case of a δ potential. This has been implemented numerically either by directly enforcing Eq. (10) or by choosing a potential of very short range. Identical results were obtained with both methods but the second one required a grid spacing small enough to resolve the fast variation of the potential. The first method was therefore preferred and has been used to generate the numerical results shown below.

We show in Fig. 8 the integration of Eq. (3) below the critical velocity starting from the $x_{0,+}$ analytical solution. The solution is seen to be stable in time. This is also obtained (data not shown) when the conservative equation (17) is replaced by the corresponding dissipative equation ($\partial_t A = -\delta K / \delta A^*$). This numerically confirms that $x_{0,+}$ solutions are local minima of K .

Figures 9 and 10 show the square modulus and phase of the solution when the initial condition is instead the $x_{0,-}$ solution. Numerical noise is sufficient to reveal the solution instability. After a transient behavior and emission of upstream and downstream propagating disturbances, the flow approaches the stable $x_{0,+}$ solution in a region around the origin which grows with time. A similar evolution was observed for all studied injection velocities less than the critical velocity (even quite close to v_c). We thus conclude that below the critical line $v_c(g)$ the flow relaxes toward the steady $x_{0,+}$ solution.

Above the critical line $v_c(g)$, no steady solution exists.

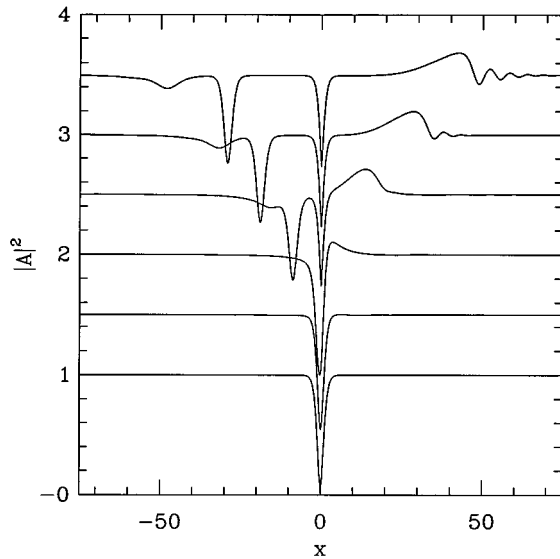


FIG. 9. Numerical integration of Eq. (3) with $v=0.3$ and $g=2$ as in Fig. 8 but starting from the steady solution (11) and (12) with $x_{0,-}=0.112\ 087$. The solution square modulus is plotted at $t=0,10,20, \dots$ up to $t=50$ (shifted upward by $t/20$). The integration shows that the initial $x_{0,-}$ solution is unstable. It emits sound and gray solitons which move upstream and downstream. Around the obstacle at $x=0$, the flow becomes time-independent and coincides with the steady $x_{0,+}$ solution.

Figures 11 and 12 show the evolution in such a case. The injection velocity is fixed at v . The initial condition is the stable steady solution corresponding to a potential strength g slightly below the critical one. At $t=0$, the potential strength is increased above the critical one. The numerical results show that waves are repeatedly emitted at the origin. Each round of emission consists of a downstream disturbance formed of a number of gray solitons (two can be

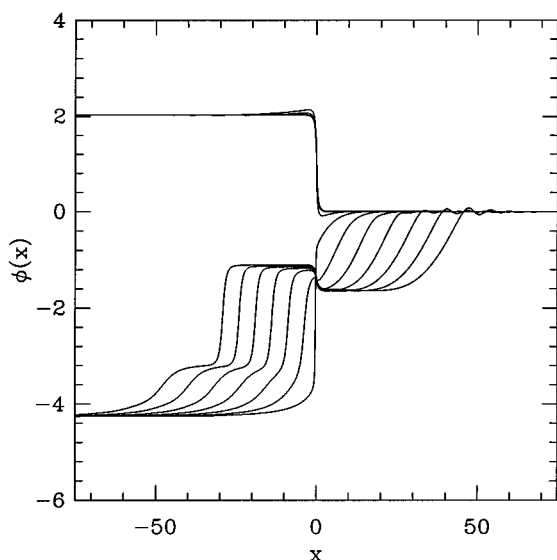


FIG. 10. The successive phases of the solution shown in Fig. 9 (but plotted twice as often). The $x_{0,+}$ solution can again clearly be seen developing around $x=0$. Note also the 2π phase jump between $t=15$ and $t=20$, which corresponds to the vanishing of the solution modulus and the emission of gray solitons.

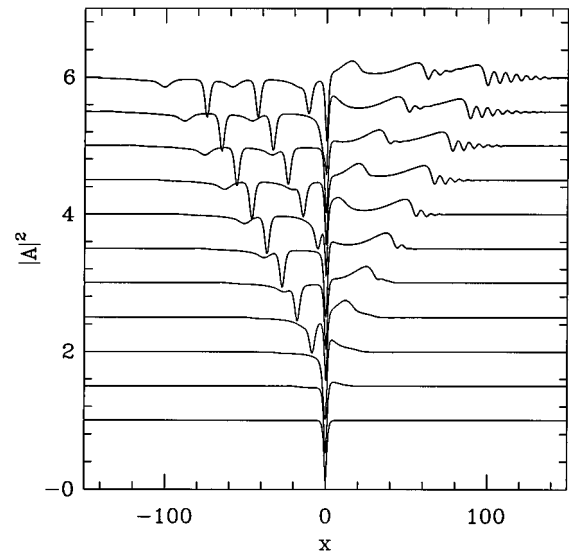


FIG. 11. Numerical integration of Eq. (3). The initial condition is the stable steady solution (11,12) for $v=0.3$ and $g=3$ ($x_{0,+}=0.345\ 377$) just below the maximum coupling $g_m=3.045\ 78$. The evolution is computed for $v=0.3$ and $g=4$ above g_m . The solution square modulus is plotted at $t=0,8,16, \dots$ up to $t=80$ (shifted upward by $t/16$). Gray solitons moving downstream and upstream moving dispersive waves are repeatedly emitted from the obstacle (three rounds of emission can actually be seen during the time period shown).

clearly seen in Figs. 11 and 12) and an upstream propagating disturbance which breaks into dispersive sound waves. For the parameter values of Figs. 11 and 12 all the emitted solitons propagate downstream faster than the injection velocity and the modulus of A vanishes at the moment of emission, as can clearly be seen from the corresponding phase jumps in

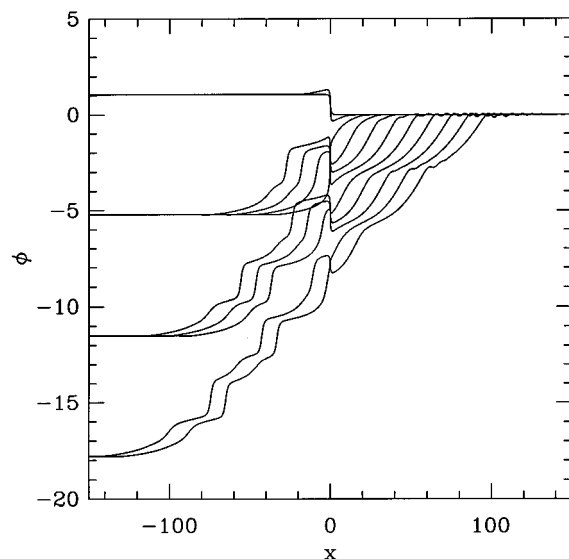


FIG. 12. The successive phases of the solution shown in Fig. 11. Note again the 2π phase jump corresponding to each emission. Here, as in the following phase plots, the phases are drawn at the same instants as the corresponding moduli. The time order of the different curves is made clear by noting that the size of the perturbed domain increases with time.

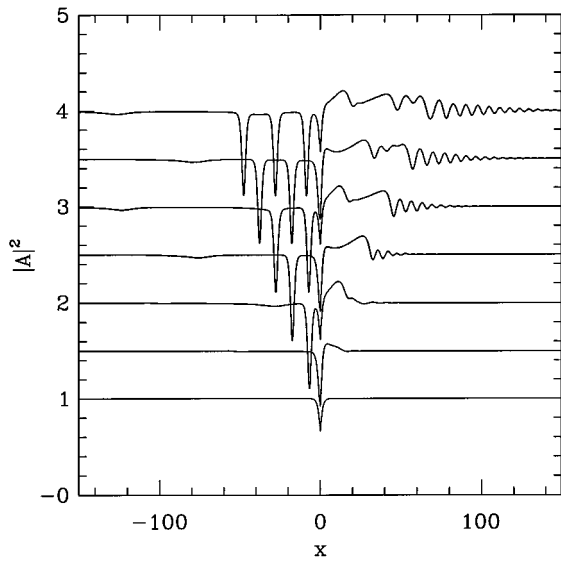


FIG. 13. Numerical integration of Eq. (3). The initial condition is the stable steady solution (11) and (12) for $v=1.0$ and $g=0.29$ ($x_{0,+}=1.30067$) just below the maximum coupling $g_m=0.30028$. The evolution is computed for $v=0.3$ and $g=0.39$ above g_m . The solution square modulus is plotted at $t=0,20,40, \dots$ up to $t=120$ (shifted upward by $t/40$). As in Fig. 11, gray solitons moving downstream and upstream moving dispersive waves are repeatedly emitted from the obstacle.

Fig. 12. For other parameter values, some solitons propagate downstream less rapidly than the mean flow and the modulus of A never vanishes, as shown in Figs. 13 and 14.

The dynamics for a general (one hump) potential appears to be qualitatively similar. We have studied potentials of Gaussian form,

$$U(x) = U_{\max} \exp[-(x/\sigma)^2]. \quad (44)$$

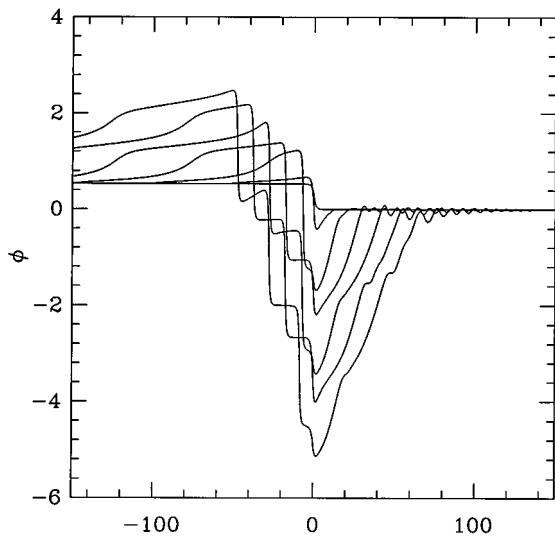


FIG. 14. The successive phases of the solution shown in Fig. 13. Note that in contrast to Fig. 12, the main soliton of each round of emission moves downstream more slowly than the injection velocity and there is no phase jump.

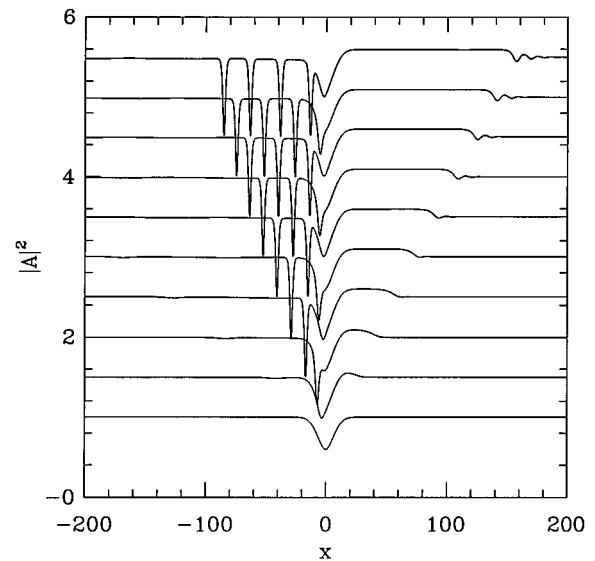


FIG. 15. Numerical integration of Eq. (3) with a potential of Gaussian form (44) with $U_{\max}=5/16, \sigma=10$. The solution square modulus is plotted at times $t=0,20,40, \dots$ up to $t=180$ (shifted upwards by $t/40$).

For $U_{\max}=g/\sqrt{\pi\sigma}$ and $\sigma \ll 1$, the results are indistinguishable from those obtained with a δ potential of strength g . Results in the other limit $\sigma \gg 1$ are presented in Figs. 15 and 16. The potential is of the form (44) with $\sigma=10$ and $U_{\max}=5/16$. The initial condition is the steady solution at an injection velocity $v=0.45$ and is very well approximated by the ‘‘adiabatic’’ solution $R(x)$ of Eq. (33) and its corresponding phase. The evolution is performed at an injection velocity of $v=0.7$ above the critical velocity $v_c \approx 0.53$ [in agreement with the estimate (43) and slightly larger than the zeroth-order approximation (34) $v_0=0.5$]. As in the δ -potential case gray solitons are repeatedly emitted and an upstream disturbance is generated. The upstream disturbance is, however, somewhat simpler than in the δ -potential case since it is of almost constant height. The flow geometry has

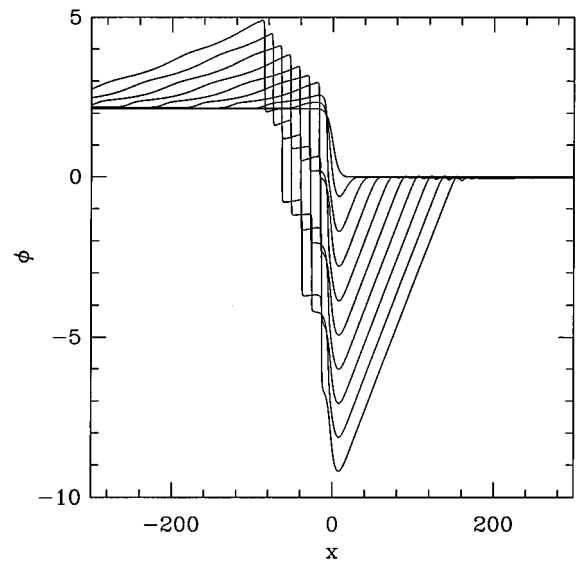


FIG. 16. The successive phases of the solution shown in Fig. 15.

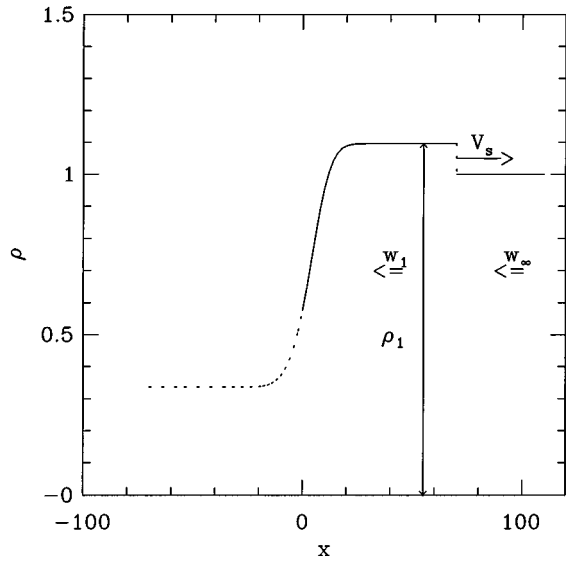


FIG. 17. Sketch of the asymptotic hydraulic solution used to interpret the results of Figs. 15 and 16.

some similarities with the classical case of a compressible fluid flow through a nozzle [20], which is itself analogous to shallow-water flow. The results are indeed reminiscent of those obtained for the flow of a stratified fluid over a localized topography (see, e.g., [21]). As in this latter context [22], the most salient features can be described by a simple ‘‘hydraulic’’ approximation which generalizes the static approximation (33) and that we now explain.

For a slowly varying potential, Eq. (3) can be rewritten to lowest order in the slow variation as

$$\partial_t \rho + \partial_x (\rho w) = 0, \quad (45)$$

$$\partial_t w + w \partial_x w + 2 \partial_x \rho + 2 \partial_x U = 0 \quad (46)$$

with boundary conditions $\rho(+\infty) = 1, w(+\infty) = -v$, where $\rho = R^2$ and $w(x) = -v + 2 \partial_x \phi$ have been introduced to emphasize the hydrodynamic analogy. This leads us to expect that above the critical velocity it is useful to consider the asymptotic ‘‘hydraulic’’ solution of Eqs. (45) and (46) depicted in Fig. 17. It consists of a critical stationary solution developing around the obstacle with an upstream depression terminated by a moving shock and a downstream depression. Of course, the shock is not a solution of the full nondissipative Eq. (3) and the singularity of Eqs. (45) and (46) is regularized instead by the development of small wavelength oscillations as previously described in the literature [23,24] and seen in Fig. 15. Similarly, the downstream depression has to be replaced by a set of gray solitons.

As in Sec. II, the profile of the stationary solution is easily derived from Eqs. (45) and (46). The conservation equation (45) determines the velocity as a function of the density and the incoming mass flux. The density profile is then obtained from Eq. (46) as

$$\frac{\rho_1^2 w_1^2}{4 \rho^2(x)} + \rho(x) + U(x) = \frac{w_1^2}{4} + \rho_1. \quad (47)$$

The criticality condition fixes a first relation [analogous to Eq. (34)] between the density ρ_1 and fluid velocity w_1 on the obstacle side of the upstream shock (see Fig. 17),

$$U_{\max} = \frac{w_1^2}{4} + \rho_1 - \frac{3}{2} (\rho_1^2 w_1^2 / 2)^{1/3}. \quad (48)$$

Two shock conditions are needed to complete the determination of ρ_1, w_1 and the shock velocity V_s as a function of the injection conditions. The determination of these analogs of the usual Rankine-Hugoniot conditions for a dissipationless shock requires a careful analysis [23] since it is *a priori* not obvious what the conserved quantities are when one traverses the expanding oscillatory shock inner structure. Here, however, we limit ourselves to cases where the injection velocity is above but close to the critical velocity v_0 , Eq. (34), where the steady flow disappears (in the hydraulic approximation). This allows us to consider only weak shocks and neglect the losses in the inner structure. Then, the conservation relations (45) and (46) across the shock give the two relations [25]

$$\begin{aligned} -V_s(\rho_\infty - \rho_1) + \rho_\infty w_\infty - \rho_1 w_1 &= 0, \\ -V_s(w_\infty - w_1) + \frac{w_\infty^2}{2} + 2\rho_\infty - \frac{w_1^2}{2} - 2\rho_1 &= 0. \end{aligned} \quad (49)$$

The fluid density ρ_∞ and velocity w_∞ on the injection side of the upstream shock are those of the undisturbed fluid at infinity, namely $\rho_\infty = 1$ and $w_\infty = -v$. For a weak shock, $\rho_1 = \rho_\infty + \delta\rho$, $\delta\rho \ll 1, w_1 = -v + \delta w$, $\delta w \ll 1$, Eq. (49) simply relates the velocity discontinuity to the density difference

$$\delta w = \sqrt{2} \delta\rho. \quad (50)$$

In the same limit, the shock velocity is found to be

$$V_s = -v + \sqrt{2} + \delta w, \quad (51)$$

which simply means that the shock is sonic relative to the downstream fluid. The critical condition (48) then determines the density increase of the upstream disturbance as a function of the small increase of the injection velocity above the critical velocity, $v = v_0 + \delta v_\infty$, $0 < \delta v_\infty \ll 1$,

$$\delta\rho = \frac{1}{\sqrt{2}} \frac{1 + (v_0^2/2)^{1/3}}{1 + (v_0^2/2)^{1/6} + (v_0^2/2)^{1/3}} \delta v_\infty. \quad (52)$$

These results can be compared with the numerical data reported in Figs. 15 and 16. The potential maximum was chosen to be $U_{\max} = 5/16$, for which the critical injection velocity is in the hydraulic approximation $v_0 = 1/2$. For an injection velocity $v = 0.7$ (i.e., $\delta v_\infty = 0.2$), Eq. (52) gives $\delta\rho = 9.6 \times 10^{-2}$, while the shock velocity and the fluid velocity decrease downstream of the shock are obtained from Eqs. (50) and (51) to be $V_s = 0.85, \delta w = 0.136$. These estimates are found to be in good agreement with the numerical data of Fig. 15 for the square modulus increase in the obstacle upstream region (which has small oscillations between $\delta\rho = 9.3 \times 10^{-2}$ and 9.6×10^{-2}) as well as for the propagation velocity of the front end of the upstream disturbance. The phase plot is quite straight in the upstream disturbance

region with a slope $\langle \partial_x \phi \rangle = 0.66$, which also agrees accurately with $\delta w/2$. Similar agreement has been observed for an injection velocity $v = 0.6$ (with the same potential). As explained in the Appendix, one can also attempt to determine the gray soliton properties (velocity, period of emission) by using the determined upstream solution and the exact laws of conservation of mass and energy through the obstacle. However, taking into account only the main gray soliton of each emission does not seem sufficient to satisfy accurately the conservation laws (especially the energy one) and does not give as satisfactory results.

IV. CONCLUSION

We have presented analytical and numerical results for the steady or time-dependent flows of a nonlinear Schrödinger fluid past an obstacle. As already mentioned, they have some similarity with the classical case of a compressible fluid flow through a nozzle and with results obtained for the flow of a stratified fluid over a localized topography [21,22,18]. Our main result is the existence of an obstacle-dependent critical velocity above which the steady flow solution disappears and gray solitons are repeatedly emitted. We have also explicitly obtained corrections to the classical criterion determining the critical velocity as the velocity for which the fluid locally reaches the sound velocity. Such corrections remain to be obtained in higher dimensions. Our study can also be developed in different directions. It would certainly be interesting to analyze wave generation more precisely. In the case of slowly varying potentials, one could, for instance, try to generalize the approach of Sec. II C to time-dependent flows in order to describe the soliton creation and determine the corrections to the hydraulic approximation. The transition from one dimension to higher-dimensional geometries is worth investigating as well as the role of gray solitons [26,27] and their analogs [28] in higher dimensions. In this case, describing the obstacle by a potential may also prove useful. Finally, the results appear potentially relevant in different physical contexts. Two, which seem particularly noteworthy, are nonlinear optics, where related observations may have already been made [29], and more speculatively, condensed atomic vapors [5], where investigations of different forms of traps and flows may become accessible in due course.

ACKNOWLEDGMENTS

I am grateful to Y. Pomeau for discussions about his work and for interesting me in this problem. I would also like to thank M. E. Brachet for instructive conversations. It is a pleasure to acknowledge the hospitality and support of the Isaac Newton Institute, Cambridge, where part of this work was carried out.

APPENDIX: CONSERVATION LAWS FOR THE NLS EQUATION WITH A POTENTIAL AND GRAY SOLITON EMISSION

The NLS equation has an infinite number of local conservation laws. At least two still exist when a potential is added as in Eq. (3). One is simply the conservation of matter which reads, in the obstacle frame,

$$\partial_t |A|^2 = \partial_x J_M \quad (\text{A1})$$

with the flux J_M given by

$$J_M = v(|A|^2 - 1) + i(A^* \partial_x A - A \partial_x A^*). \quad (\text{A2})$$

The other derives from the conservation of the Hamiltonian K (17),

$$\partial_t (\mathcal{H} - v\mathcal{P}) = \partial_x J_K \quad (\text{A3})$$

with the energy density \mathcal{H} and momentum density \mathcal{P} defined as in Eq. (19),

$$\begin{aligned} \mathcal{H} &= |\partial_x A|^2 + \frac{1}{2}(|A|^2 - 1)^2 + U(x)(|A|^2 - 1) \\ \mathcal{P} &= \frac{1}{2i}(A^* \partial_x A - A \partial_x A^*) \end{aligned} \quad (\text{A4})$$

and the flux J_K ,

$$\begin{aligned} J_K &= i\{\partial_{xx} A \partial_x A^* - \partial_{xx} A^* \partial_x A + (A \partial_x A^* - A^* \partial_x A) \\ &\quad \times [1 - |A|^2 - U(x) - v^2/2]\} \\ &\quad - v\{-2|\partial_x A|^2 + 1/2(A^* \partial_{xx} A + A \partial_{xx} A^*) \\ &\quad + |A|^2 - |A|^4 - U(x)|A|^2\}. \end{aligned} \quad (\text{A5})$$

Since the mass, momentum, and energy contained in any finite interval of space are bounded, the time-averaged fluxes $\langle J_M(x) \rangle$ and $\langle J_K(x) \rangle$ should be independent of the space position x . For a slowly varying potential, the value of these fluxes upstream of the obstacle can be determined from the hydraulic approximation, which gives

$$\begin{aligned} J_M^{(\text{hydr.})} &= v(\rho_1 - 1) - (w_1 + v)\rho_1 \approx (v - \sqrt{2})\delta\rho, \\ J_K^{(\text{hydr.})} &= -\rho_1(w_1 + v)^3/4 + \rho_1(w_1 + v)(1 - \rho_1 - v^2/2) \\ &\quad - \rho_1 v[-3(w_1 + v)^2/4 + 1 - \rho_1] \\ &\approx v\delta\rho(1 - v/\sqrt{2}). \end{aligned} \quad (\text{A6})$$

Downstream of the obstacle, it is the passage of gray solitons which gives nonzero values to the time integrals of J_M and J_K . Assuming that the solitons are well separated, this gives

$$\begin{aligned} \int_0^t dt J_M(x, t) &= -2 \sum \sqrt{2 - (v + w_{gs})^2}, \\ \int_0^t dt J_K(x, t) &= \sum \left\{ \frac{2}{3} [2 - (v + w_{gs})^2]^{3/2} \right. \\ &\quad \left. + v(v + w_{gs}) \sqrt{2 - (v + w_{gs})^2} \right\}^2, \end{aligned} \quad (\text{A7})$$

where the sum is over all solitons which have passed through x between 0 and t (w_{gs} is the velocity in the obstacle frame of the considered soliton).

It can be attempted to satisfy Eq. (A7) by taking into account only the main soliton of each emission. This gives two equations for the period of emission T and the velocity w_s of the emitted solitons

$$T\delta\rho(\sqrt{2}-v)=2\sqrt{2-(v+w_{gs})^2}, \quad (\text{A8})$$

$$T\delta\rho(\sqrt{2}-v)v/\sqrt{2}=\frac{2}{3}[2-(v+w_{gs})^2]^{3/2} \\ +v(v+w_{gs})\sqrt{2-(v+w_{gs})^2}. \quad (\text{A9})$$

For an injection velocity $v=0.7$ one obtains $T=39.9, w_{gs}=-1.06$ to be compared to the simulation values $T\approx 42, w_{gs}\approx -0.6$. While the prediction is satisfactory for the period, it is quite imprecise for the gray soliton velocity, which is small in the fluid referential frame ($|v+w_{gs}|\ll 1$). The main defect of the approximation appears to come from the neglect of the small solitons, which contributes negligibly to the mass balance but quite significantly to the balance of energy. In fact, good results are obtained by assuming $v+w_{gs}\approx 0$ and using only Eq. (A8).

-
- [1] V. I. Talanov, Pis'ma Zh. Éksp. Teor. Fiz. **2**, 31 (1965) [JETP Lett. **2**, 141 (1965)]; A Hasegawa and F. Tappert, Appl. Phys. Lett. **23**, 142 (1973); **23**, 171 (1973).
- [2] H. Hasimoto and H. Ono, J. Phys. Soc. Jpn **33**, 805 (1972). Note, however, that in this case the nonlinear term is attractive in contrast to the case studied here.
- [3] L. P. Pitaevskii, Zh. Éksp. Teor. Fiz. **40**, 640 (1961) [Sov. Phys. JETP **13**, 451 (1961)]; E. P. Gross, Nuevo Cimento **20**, 454 (1961).
- [4] A. Griffin *et al.*, *Bose-Einstein Condensation* (Cambridge University Press, Cambridge, 1995).
- [5] M. H. Anderson *et al.*, Science **269**, 198 (1995); C. C. Bradley *et al.*, Phys. Rev. Lett. **75**, 1687 (1995); K. B. Davis *et al.*, *ibid.* **75**, 3969 (1995).
- [6] T. Frisch, Y. Pomeau, and S. Rica, Phys. Rev. Lett. **69**, 1644 (1992).
- [7] Y. Pomeau and S. Rica, C. R. Acad. Sci. (Paris) II **311**, 1523 (1993); Phys. Rev. Lett. **71**, 247 (1993); **72**, 2426 (1994).
- [8] M. Stone and A. M. Srivastava, J. Low Temp. Phys. **102**, 445 (1996).
- [9] G. G. Nancolas *et al.*, Nature **316**, 797 (1985); P. V. E. McClintock, Z. Phys. B **98**, 429 (1995).
- [10] J. C. Saut has kindly informed us that solutions of the focusing nonlinear Schrödinger equation with a potential have been analyzed in the literature [see, e.g., Y. G. Oh, Commun. Math. Phys. **131**, 223 (1990), and references therein]. In the focusing case with boundary condition $A=0$ at $x=+\infty$, the impurity motion does not bring anything new since it can be gotten rid of by a Galilean transformation into the moving frame of the impurity.
- [11] T. Tsuzuki, J. Low Temp. Phys. **4**, 441 (1971).
- [12] V. E. Zakharov and A. B. Shabat, Zh. Éksp. Teor. Fiz. **64**, 1627 (1973) [Sov. Phys. JETP **37**, 823 (1973)].
- [13] If desired, the term $v\partial_x A$ can be eliminated by using instead of A a rotating field $B(x,t)=\exp[i(-vx/2+v^2t/4)]A(x,t)$.
- [14] The analogy between NLS flow and conventional hydrodynamics is pursued in C. Nore *et al.*, Physica D **65**, 154 (1993); C. R. Acad. Sci. (Paris) II **319**, 733 (1994).
- [15] The merging value is given by $x_{0,m}=(2/\sqrt{2-v^2})\tanh^{-1}\sqrt{(1+4v^2)^{1/2}-(1+v^2)/2-v^2}$.
- [16] The necessity of adding this term for constant flow has been noted previously [see, e.g., P. W. Anderson, Rev. Mod. Phys. **38**, 298 (1966)]. It plays an important role in the computation since without it the steady solutions of Eq. (3) would not even be stationary points of K . Sometimes, this supplementary term is included in the momentum definition giving the so-called "renormalized momentum" [see, e.g., I. V. Barashenkov and E. Yu. Panova, Physica D **69**, 114 (1993); I. M. Uzunov and V. S. Gerdjikov, Phys. Rev. A **47**, 1582 (1993)].
- [17] F. Klinkhamer and N. Manton, Phys. Rev. D **30**, 2212 (1984).
- [18] This can also be obtained by remembering that the small amplitude limit of the defocusing NLS gives the Korteweg-de Vries (KdV) equation [see, e.g., V. E. Zakharov and E. A. Kuznetsov, Physica D **18**, 455 (1986)]. The result for the pinning of a KdV soliton by a moving δ' perturbation [B. A. Malomed, Physica D **32**, 393 (1988)] then gives back Eq. (15). One can also note that Eq. (30) is the integrated form of the corresponding stationary KdV equation.
- [19] For $|\Delta|\gg 1$, the nature of the two solutions is best seen with the variables $y=X/\sqrt{|\Delta|}$ and $\sigma=\rho/\sqrt{|\Delta|}$, for which the small parameter $|\Delta|^{-3/2}$ appears in front of the derivative term.
- [20] L. D. Landau and E. M. Lifshitz, *Fluid Mechanics* (Pergamon Press, Oxford, 1987).
- [21] T. R. Akylas, J. Fluid Mech. **141**, 455 (1984); T. Y. Wu, *ibid.* **184**, 75 (1987); S. J. Lee *et al.*, *ibid.* **199**, 569 (1989), and references cited therein.
- [22] P. G. Baines, J. Fluid Mech. **146**, 127 (1984); R. H. J. Grimshaw and N. Smyth, *ibid.* **169**, 429 (1986).
- [23] A. V. Gurevich and L. P. Pitaevski, Zh. Éksp. Teor. Fiz. **65**, 590 (1973) [Sov. Phys. JETP **38**, 291 (1974)]; A. V. Gurevich and A. L. Krylov, *ibid.* **92**, 1684 (1987) [*ibid.* **65**, 944 (1987)].
- [24] B. Fornberg and G. B. Whitham, Philos. Trans. R. Soc. A **289**, 373 (1978); S. Jin, C. D. Levermore, and D. W. McLaughlin, in *Singular Limits of Dispersive Waves*, edited by N. Ercolani *et al.*, NATO ARW Series (Plenum, New York, 1992).
- [25] Note that away from the weak shock limit, inequivalent conditions would result from using different conservation laws. This would, for example, be the case if the momentum conservation equation $\partial_t(\rho v)+\partial_x(\rho v^2+\rho^2)$ [which follows from adding Eqs. (45) and (46)] was used instead of Eq. (46).
- [26] E. A. Kuznetsov and S. K. Turitsyn, Zh. Éksp. Teor. Fiz. **94**, 119 (1988) [Sov. Phys. JETP **67**, 1583 (1988)]; E. A. Kuznetsov and J. J. Rasmussen, Phys. Rev. E **51**, 4479 (1995).
- [27] C. Josserand and Y. Pomeau, Europhys. Lett. **30**, 43 (1995).
- [28] C. A. Jones, S. J. Putterman, and P. H. Roberts, J. Phys. A **19**, 2991 (1986).
- [29] M. Vaupel, K. Staliunas, and C. O. Weiss, Phys. Rev. A **54**, 880 (1996).